

# Rapid detection of urokinase plasminogen activator using flexible paper-based graphene-gold platform

SCI F

Cite as: Biointerphases 15, 011004 (2020); doi: 10.1116/1.5128889

Submitted: 23 September 2019 · Accepted: 9 January 2020 ·

Published Online: 4 February 2020



View Online



Export Citation



CrossMark

Bipin Sharma, Prakash Parajuli, and Ramakrishna Podila<sup>a)</sup>

## AFFILIATIONS

Department of Physics and Astronomy, Laboratory of Nano-Biophysics, Clemson Nanomaterials Institute, Clemson University, Clemson, South Carolina 29634

<sup>a)</sup>Electronic mail: [rpodila@g.clemson.edu](mailto:rpodila@g.clemson.edu)

## ABSTRACT

Many studies have shown that urokinase plasminogen activator (uPA) is causally involved in promoting cancer invasion and metastasis. Thus, monitoring uPA levels could be very useful in cancer diagnosis, identification of initial metastasis, and guiding cancer treatment. Here, the authors developed a novel and scalable uPA sensor based on a graphene-gold nanoparticle platform that uses fluorescence of quantum dots to rapidly (<1 h) detect uPA up to 100 pM. Indeed, the authors' sensor is highly selective and showed an ability to sense up to 100 pM uPA even in the presence of complex biological milieu such as the fetal bovine serum.

Published under license by AVS. <https://doi.org/10.1116/1.5128889>

## I. INTRODUCTION

The majority of the cancer-related (>90%) deaths are usually caused due to the metastatic spread of tumor cells.<sup>1–3</sup> Despite the emergence of efficient therapeutic strategies to treat primary tumors in recent years, targeting tumor metastasis has not been very successful. A major event in metastasis is the proteolytic degradation of the extracellular matrix that leads to tumor cell invasion, migration, and homing to other organs. Although many protease systems are suspected to be involved in metastasis, several studies have shown that urokinase plasminogen activator (uPA) is causally involved in promoting cancer invasion and metastasis. Particularly, elevated expression of the components of the uPA system has been correlated with adverse patient outcomes in multiple types of cancer (e.g., breast, prostate, colorectal, etc.).<sup>1,4–8</sup> In the case of prostate cancer cells, Bekes *et al.*<sup>9</sup> found that uPA participates at an early phase in the initial escape of tumor cells from the primary site. Duffy *et al.*<sup>4</sup> suggested that monitoring uPA levels could be very helpful in determining the course of treatment in breast cancer patients. Similarly, uPA also has been proposed for monitoring multiple cancer types including prostate cancer.<sup>1–9</sup>

According to the World Health Organization (WHO), cancer is the second leading cause of death globally and is responsible for

an estimated 9.6 million deaths in 2018 alone.<sup>10</sup> Among 9.6 million deaths, ~70% occurred in low- and middle-income countries due to the lack of access to rapid, inexpensive, and point-of-care diagnostic sensors that could be used in a resource-limited setting. According to WHO, in 2017, only 26% of low-income countries reported having pathology services generally available in the public sector. In this regard, there is a great need to develop novel inexpensive sensors that could rapidly diagnose biomarkers such as uPA to improve cancer treatment globally.

Graphene is an ideal platform for biosensing due to its high surface area and unique physicochemical properties. Indeed, graphene biosensors have been used in various modes ranging from electrical/electrochemical to optical detection for sensing a variety of analytes.<sup>11–19</sup> Graphene-based materials (e.g., graphene, graphene oxide, carbon nanotubes, etc.) exhibit excellent fluorescence quenching<sup>20,21</sup> due to nonradiative resonant energy transfer associated with the  $\pi$ -electron cloud. Similarly, noble metal nanoparticles exhibit surface plasmon resonance (SPR) in the visible spectrum.<sup>22,23</sup> SPR enhances the local electric field, which can induce an increase in quantum yield of fluorescent dyes and quantum dots (QDs) within its vicinity. Building on SPR and fluorescence quenching of graphene, we fabricated a novel graphene-Au nanoparticle (NP) sensing platform on cellulose-based paper for highly

selective sensing of uPA. Using this platform, we achieved a sensitivity as low as 100 pM for uPA even in the presence of complex fluids such as fetal bovine serum (FBS). Unlike many existing carbon nanomaterial assays with low sensitivity ( $\sim 50$  nM<sup>24</sup>) or long incubation times, uPA sensing using graphene-Au NP platform is very rapid (<1 h), highly reliable, inexpensive, and easily scalable.

## II. EXPERIMENT

### A. Fabrication of graphene-Au NP paper

Exfoliated graphene nanoplatelets (Grade M) were obtained from XG Science (Mason, MI). Detailed atomic force and scanning electron microscopy images of graphene platelets are provided in the supplementary material (Figs. S1 and S2).<sup>36</sup> A 5 mg/ml suspension of exfoliated graphene nanoplatelets was prepared in 75 ml acetone via tip sonication for 30 min (Branson 250W, 1/8 in. tip sonicator). This solution was then spray-coated onto an A4 printer paper thrice using an industrial spray gun (Iwata 5095WS400; 1.3 mm nozzle, 29 psi ambient air pressure). During the last coat, 7.5 ml of 1.5 mg/ml  $\sim 10$  nm Au NPs (Vive Nano, Inc.) was added a coat to obtain a uniform layer of graphene-Au NPs on a standard copier paper. This corresponds to a net areal Au NP density of  $\sim 18 \mu\text{g}/\text{cm}^2$ , which was found to be optimal for sensing based on our previous studies.<sup>25</sup> Transmission electron microscopy images of Au NPs are provided in the supplementary material (Fig. S3).<sup>36</sup> The paper was dried for 15 min in air after each coating. The dried graphene-Au NP papers were stored in dark and dry conditions.

### B. Preparation of standard buffer

The standard buffer to be used as the solvent for all the experimental studies was prepared by mixing 0.5% (v/v) Tween-20 and 1% (w/v) of Bovine Serum Albumin (BSA) in 0.01M phosphate buffer saline.

### C. Conjugation of CdSe quantum dots with uPA antibodies

A mixture was prepared with a final concentration of 100 nM for CdSe QDs (Thermo Fisher Scientific-Invitrogen, Cat #Q10123MP) and 200  $\mu\text{g}/\text{ml}$  for uPA Ab (Abcam, Lot # GR131433) in the standard buffer. This mixture was then placed on a shaker at 650 rpm at 4 °C for 60 min to ensure the conjugation of antibodies (Abs) to QDs. These optimal concentrations for QDs and Ab were chosen based on previous studies with other analytes similar to uPA.<sup>25,26</sup> In this case, the binding of Ab on CdSe QDs is nonspecific and is primarily governed by ionic, van der Waals, and hydrophobic forces.<sup>26–28</sup>

### D. Preparation of graphene-Au NP sensing platform

The graphene-Au NP paper was cut into  $\sim 1 \text{ cm}^2$  pieces for sensing experiments, and 2  $\mu\text{l}$  of the uPA Ab-conjugated QDs was drop casted on to  $1 \text{ cm}^2$  graphene-Au NP paper and left for drying under ambient conditions for around 1 h. Upon drying, the fluorescence intensity of QDs was measured using a Renishaw InVia micro-spectrometer equipped with a 532 nm laser. The fluorescence intensity was collected from multiple spots per sample (at least three different spots) with at least three different replicates ( $n = 3$ ).

A comparison of QD fluorescence on papers with and without graphene is shown in the supplementary material (Fig. S4).<sup>36</sup>

### E. Using the sensing platform for uPA antigen detection

Recombinant human uPA protein (Abcam, Lot #GR314499) solution in different concentrations (100 pM–1  $\mu\text{M}$ ) was prepared by dissolving the uPA protein in the standard buffer. Another set of concentrations (100 pM–100 nM) was prepared in FBS for the interference study to investigate the selectivity of our assay. All the solutions were stored at 4 °C. For sensing experiments, 20  $\mu\text{l}$  of uPA solution of different concentrations (in either standard buffer or FBS) was added to the QD-Ab coated on graphene-Au NP paper. The solutions made in the standard buffer took around 20 min to dry while those made in FBS took around 60 min. Once dry, the fluorescence emission was measured for at least three separate spots using a Renishaw InVia micro-spectrometer at 532 nm. All the data shown in this work are the average fluorescence collected from multiple spots (at least three) to avoid artifacts arising from the inhomogeneous distribution of the antibody/antigen.

## III. MODELING

### A. Density functional theory

A density functional theory (DFT) calculation with DFT-D2 approach was used to calculate charge transfer between graphene and CdSe QDs. DFT-D2 is a first-principles calculation based on DFT with van der Waals corrections, which is explained in detail in Refs. 29–31. The calculations were performed using the Quantum ESPRESSO code with ultrasoft pseudopotentials for a plane wave basis set within generalized gradient approximation with the Perdew Burke-Ernzerhof exchange correlation functional including London dispersion. Before stacking up two systems to calculate the charge transfer, each system (viz., graphene and CdSe) was individually optimized to obtain correct parameters such as cell dimensions, k-mesh, and energy cutoff for the plane wave basis. After obtaining the right parameters, the two systems were stacked over one another with a  $7 \times 7$  supercell size (98 carbon atoms) for graphene matching  $4 \times 4$  supercell size (16 Cd atoms and 16 Se atoms) for the CdSe system. The energy expense of matching two supercells together was within the optimization threshold for energy of  $10^{-4}$  Ry. Due to high computational cost, the CdSe bulk structure was approximated to a single layer to be stacked over the graphene layer and relaxed for optimization.

## IV. RESULTS AND DISCUSSION

The operation mechanism of our graphene-Au NP platform is described in Fig. 1. The original fluorescence of CdSe QDs in the QD-antibody (QD-Ab) complex is quenched by graphene due to the interaction between the  $\pi$ -electron cloud of graphene and CdSe QDs. Upon the addition of an analyte (i.e., uPA in this case), the analyte binds with an antibody (Ab) on QDs raising QDs above graphene paper. In other words, as shown in Fig. 1(d), antigen-Ab acts as a spacer between graphene and the QD-Ab ensuring the reappearance of the fluorescence of QDs. The fluorescence of QDs

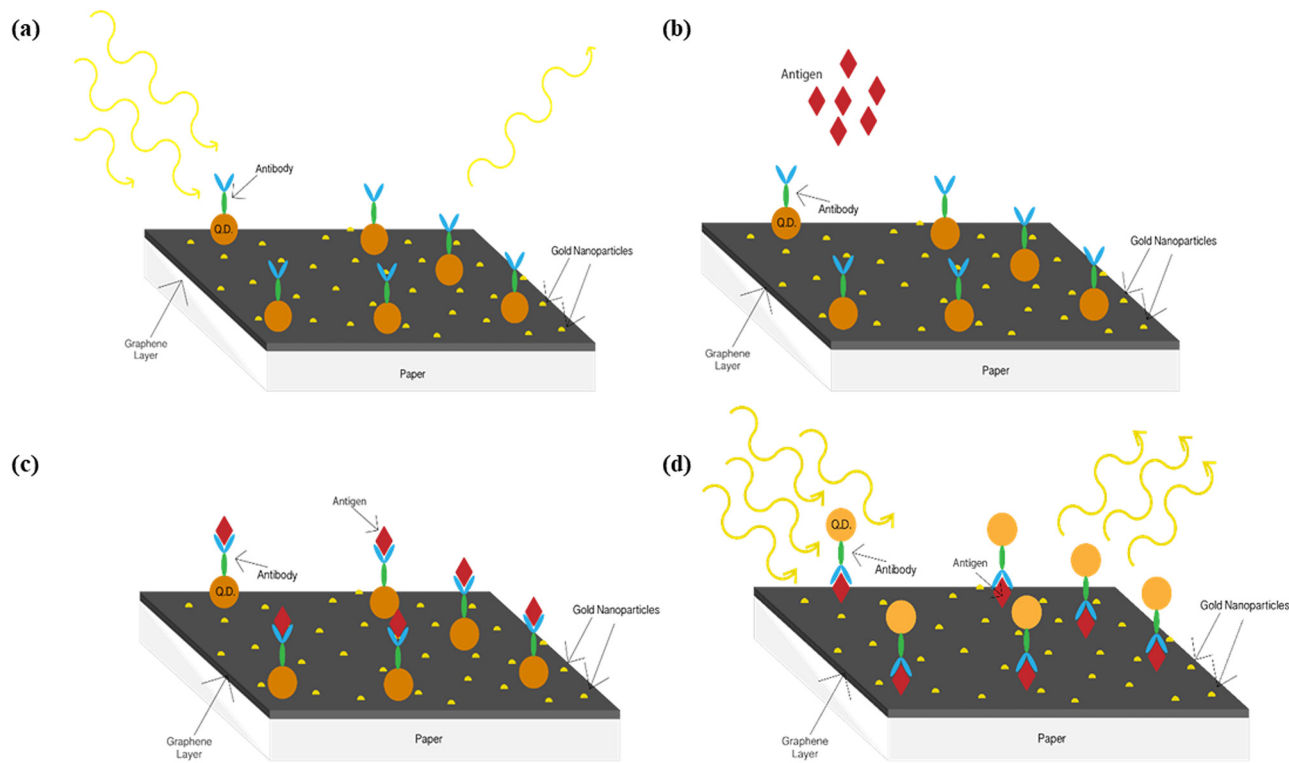


**FIG. 1.** (a) Sensing platform consists of receptor (uPA antibody) functionalized CdSe QDs deposited on a cellulose paper coated with graphene. The fluorescence emission from CdSe QDs is quenched when QDs are spatially close to graphene. (b) Upon the addition of an analyte (e.g., uPA protein), some CdSe QDs are lifted off from the graphene surface due to binding with the antibodies on the surface of CdSe QDs. The binding increases the spatial gap between CdSe QDs and graphene, which disrupts the quenching and thereby results in an increased emission from QDs. (c) and (d) Number of CdSe QDs lifted off from graphene surface is proportional to the analyte concentration. The plasmonic Au NPs enhance the emission of CdSe QDs. Thus, the increase in the emission of CdSe QDs could be used as a tool to enable highly sensitive detection of low analyte concentrations.

lifted off the surface by the analyte is further enhanced by the presence of the Au NPs leading to high sensitivity.

Our DFT calculations showed that graphene-CdSe form a charge transfer complex when they are in close vicinity, which leads to nonradiative fluorescence quenching. The charge transfer profile is shown in Figs. 2(a)–2(c). While the darker (blue in online image) regions show the area from where the charge is removed, the lighter (red in online image) regions represent regions of charge accumulation. The charge transfer profile along the  $z$ -axis (perpendicular to graphene and CdSe system plane) is shown in Fig. 2(d) with graphene at  $z=0$  plane. The shaded area was integrated to obtain the total amount of the charge transfer from graphene to the CdSe layer, which was about  $0.18\text{ e}$ . This charge transfer complex between graphene-CdSe plausibly results in the quenching of CdSe fluorescence (see Fig. 2).

The quantum yield ( $Q$ ) of a fluorophore (CdSe in this case) in the presence of a quencher (graphene in this case) can be expressed as<sup>32</sup>

$$Q = \frac{\Gamma}{\Gamma + \Gamma_{Qu} + k_{nr}}, \quad (1)$$

where  $\Gamma$  is the radiative decay rate,  $\Gamma_{Qu}$  is the nonradiative decay rate arising due to the charge transfer complex between graphene and QDs, and  $k_{nr}$  is the inherent nonradiative decay rate of CdSe QDs. Upon raising QDs from the surface of graphene, the effects of  $\Gamma_{Qu}$  become weaker. This leads to an overall increase in the quantum yield. Furthermore, in the presence of Au NPs, the quantum yield of the QDs can be expressed as

$$Q = \frac{\Gamma + \Gamma_m}{\Gamma + \Gamma_m + \Gamma_{Qu} + k_{nr}}, \quad (2)$$

where  $\Gamma_m$  is the change in the radiative decay rate due to the presence of Au NPs. When the QDs are raised from the graphene surface in the presence of Au NPs, a positive  $\Gamma_m$  further increases fluorescence when the fluorophore is 5–20 nm away from the Au NPs.<sup>32–35</sup> When uPA is added to QD-Ab complex on graphene-Au NP paper, it binds with the uPA antibody on QDs to form a graphene-QD-Ab-uPA complex, which raises QDs above the graphene surface. To test the quenching efficiency of graphene, we drop casted  $2\mu\text{l}$  of the QD-Ab simultaneously on a normal paper and on the graphene-Au NP paper.

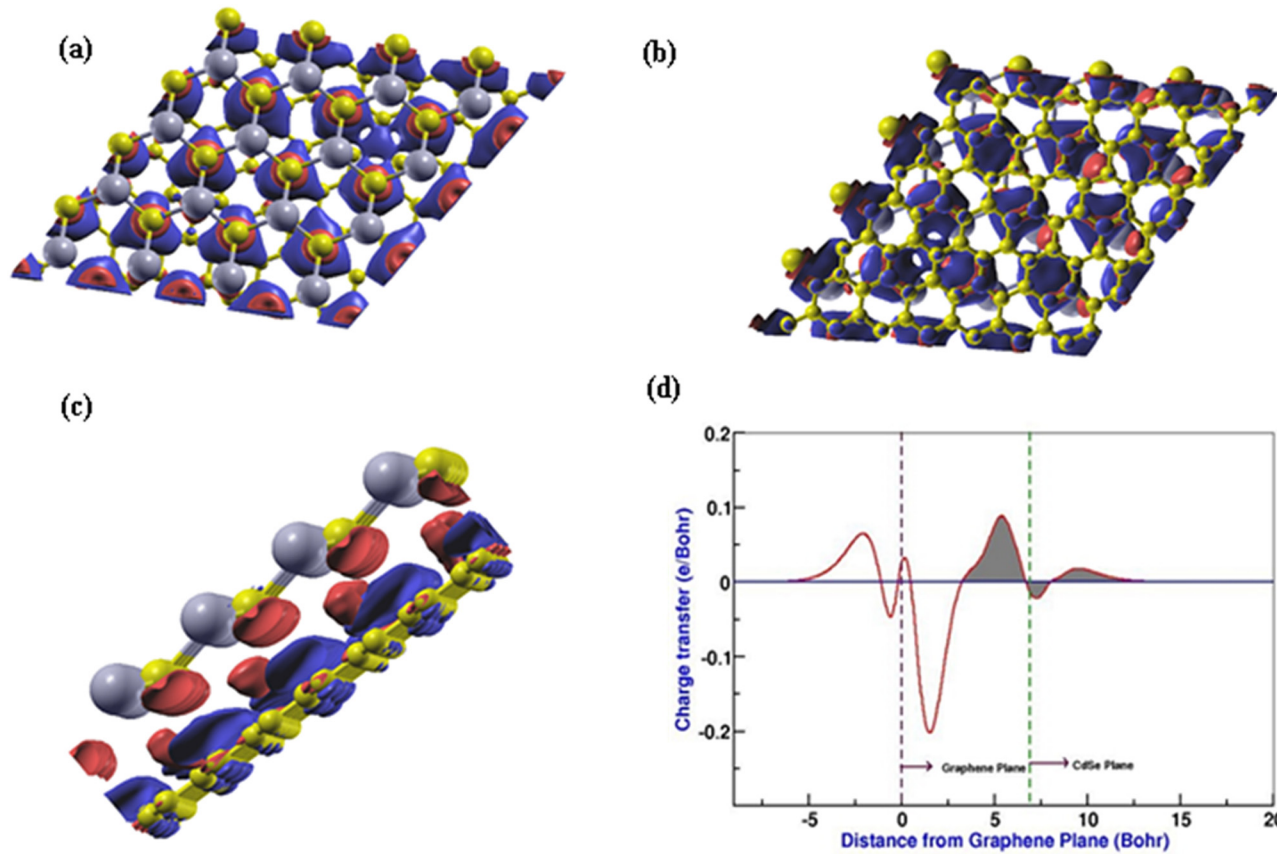


**FIG. 2.** DFT calculation to evaluate the charge transfer between graphene and CdSe. (a) Top-view with CdSe on top. (b) Top-view with graphene on top. (c) Side view for 3D charge transfer pattern. Blue (or red) regions (see color image online) represent areas with charge depletion (or accumulation). (d) Charge transfer profile along the z-axis. The area under shade was integrated to get the total amount of charge transfer from graphene to CdSe layer and was about 0.18 e.

As expected, a significant decrease was observed in the emission intensity of QDs on graphene-Au NP paper (Fig. S4 in the supplementary material).<sup>36</sup> This fluorescence intensity of the graphene-QD-Ab was used as the control intensity. A concentration study was performed with different concentrations of uPA protein ranging from 100 pM to 1  $\mu$ M in the standard buffer solution. As shown in Fig. 3(a), a gradual increase is evident in the fluorescence intensity with the increasing concentration of the uPA protein. These intensities are plotted in Fig. 3(b), which displays experimentally recorded average fluorescence intensities (recorded from at least three sampling spots) for different concentrations of uPA. As it can be deduced from Fig. 3(b), concentrations as low as 100 pM of uPA can be detected using this method.

The selectivity of our assay was evaluated using proteins other than uPA such as apolipoprotein A-1 (Apo A-1) and immunoglobulin G (IgG) [Figs. 3(c) and 3(d)]. For the selectivity study, 1 nM (which is an order of magnitude above our detection limit of 100 pM for uPA) solutions of IgG and Apo A-1 proteins were prepared in the standard buffer. Figure 3(c)

shows the average fluorescence intensities recorded after the addition of the IgG and Apo A-1 solutions, respectively. As evident from these results, there was no increase in the emission upon the addition of the IgG or Apo A-1 proteins even at a concentration as high as 1 nM. The uPA antibody is highly selective and thus it does not bind with these proteins (IgG and Apo A-1) and thus eliminates the possibility of formation of a spacer between the QDs and graphene.

In order to further evaluate the selectivity of our sensing platforms, solutions of different concentrations of uPA protein were prepared in FBS instead of the standard buffer. FBS is a complex mixture of many proteins and lipids and is often used as a serum supplement for *in vitro* culturing of eukaryotic cells. Accordingly, detection in FBS is more complex due to the presence of a variety of other proteins and molecules that are similar to uPA in size and structure. Given that our sensing platform is based on the binding of the analyte with the uPA antibodies, we expected that the sensitivity of our platform to not change significantly even in the presence of any interfering molecules. Indeed, as shown in Fig. 3(d), a steady increase in the fluorescence intensity was observed with

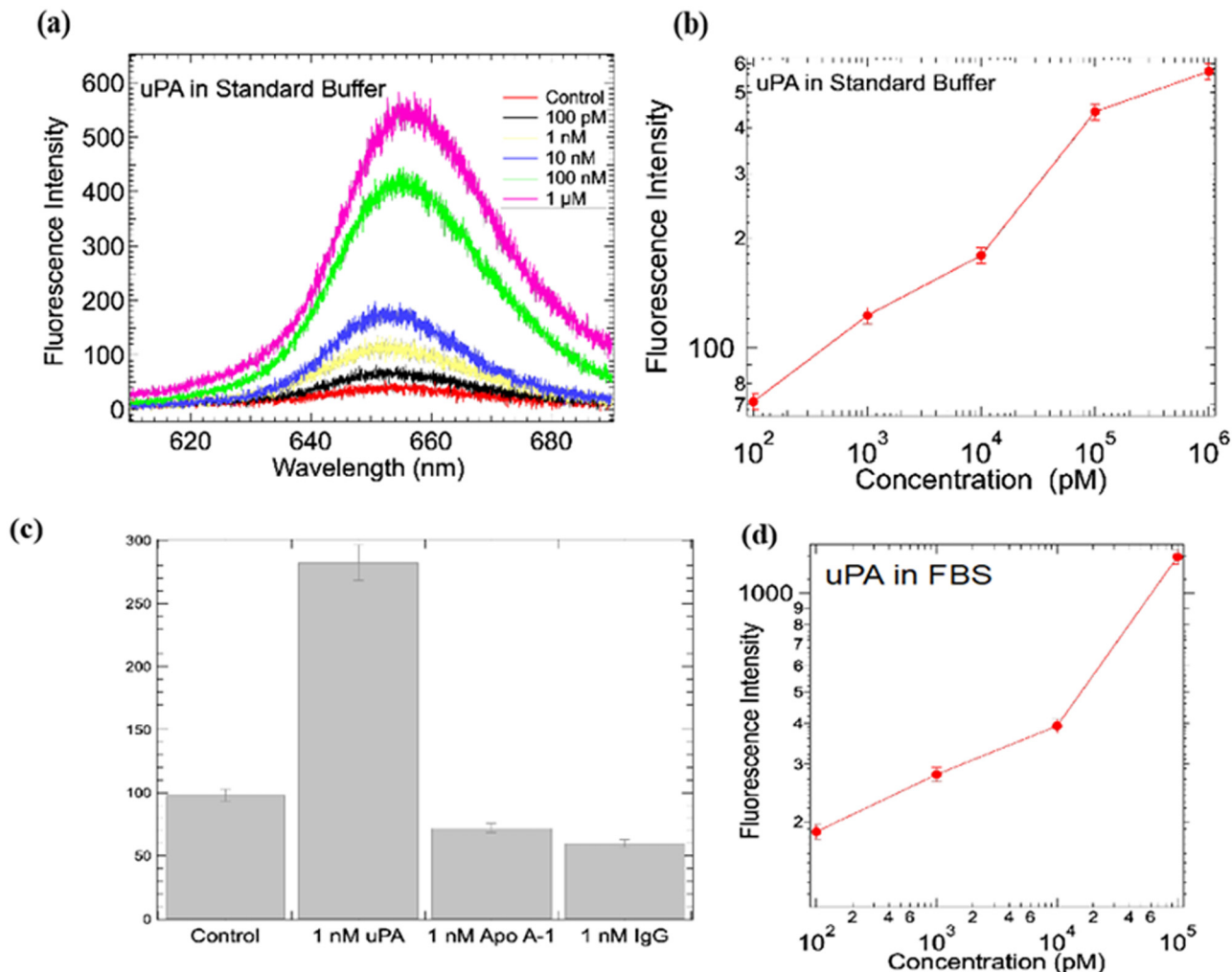


**FIG. 3.** (a) Emission intensities of uPA antibody coated CdSe QDs on graphene-Au NP paper. The emission intensity before the addition of uPA protein is labeled as the control. The addition of uPA protein leads to the raising of the QDs from the surface of graphene, leading to an increase in the fluorescence intensity. (b) Plot showing the dependence of fluorescence intensity on the concentration of uPA. Both these measurements were performed with the standard buffer as the solvent for the uPA antigen. (c) Fluorescence intensities obtained by addition of 1 nM of different biomolecules in standard buffer to CdSe QDs coated with uPA antibody. The emission intensity before the addition of any biomolecule is labeled as the control. The addition of uPA protein causes an increase in fluorescence intensity while there is almost no significant change in the fluorescence intensity upon addition of nonspecific proteins. (d) Fluorescence intensities of different concentrations of uPA in FBS. There is a clear trend of increasing fluorescence with increasing uPA concentrations suggesting that our platform can sense uPA even in the presence of a complex milieu containing a wide variety of proteins and lipids.

increasing concentration of uPA in FBS similar to the case of standard buffer confirming the selectivity of our platform.

Lastly, it should be mentioned that our platforms are at least an order of magnitude cheaper than existing ELISA platforms for uPA. Considering that we use  $\sim 1.25 \text{ mg/cm}^2$  of Au NPs and  $\sim 1\text{--}5 \text{ mg/cm}^2$  of graphene ( $\sim \$450/\text{kg}$  for graphene and  $\$384\,000/\text{kg}$  for Au), the price of a  $1 \text{ cm}^2$  sensing platform coupon is  $\sim \$0.5$ . Thus, one can fabricate 100 such platforms for  $\$50$ , which is significantly inexpensive (by an order of magnitude) compared to a standard uncoated 96-well plate uPA ELISA kit ( $\sim \$539$ ).

## V. SUMMARY AND CONCLUSIONS

Graphene-Au NP paper was used as a sensing platform for the detection of uPA protein. CdSe QDs coated with uPA antibody showed extremely low fluorescence emission when deposited on the graphene-Au NP paper due to fluorescence quenching. Our DFT calculations suggested that such quenching plausibly arises from charge transfer between graphene and CdSe QDs. The graphene-Au NP platform was able to achieve up to 100 pM uPA sensitivity in the standard buffer. The selectivity of the sensing platform was also evaluated

using Apo A-I, IgG, and FBS. No discernible effects of the interfering proteins were observed on the detection of uPA. Although other platforms such as ELISA may provide similar sensitivities, the graphene-Au NP platform is inexpensive, flexible, and rapid ( $\sim 1$  h). One main advantage of a flexible sensor is that it can be wrapped or pressed more easily against the patients' fingers to absorb the blood from a simple needle prick similar to existing glucose sensors available in the market. This opens up the possibility of the creation of handheld and point-of-care sensors for low- and middle-income countries.

## ACKNOWLEDGMENTS

R.P. acknowledges the Clemson University for providing start-up funds. R.P. also acknowledges support from NIHR01ES019311-07. The authors would also like to thank Ms. Courtney Stewart for her valuable input in this work.

## REFERENCES

- <sup>1</sup>N. Mahmood, C. Mihalcioiu, and S. A. Rabbani, *Front. Oncol.* **8**, 24 (2018).
- <sup>2</sup>P. Mehlen and A. Puisieux, *Nat. Rev. Cancer* **6**, 449 (2006).
- <sup>3</sup>B. Weigelt, J. L. Peterse, and L. J. van't Veer, *Nat. Rev. Cancer* **5**, 591 (2005).
- <sup>4</sup>M. J. Duffy and C. Duggan, *Clin. Biochem.* **37**, 541 (2004).
- <sup>5</sup>M. J. Duffy, *Clin. Chem.* **48**, 1194 (2002).
- <sup>6</sup>S. J. Shin, K. O. Kim, M. K. Kim, K. H. Lee, M. S. Hyun, K. J. Kim, J. H. Choi, and H. S. Song, *Jpn. J. Clin. Oncol.* **35**, 342 (2005).
- <sup>7</sup>H. Taubert *et al.*, *Br. J. Cancer* **102**, 731 (2010).
- <sup>8</sup>H. Pappot, A. N. Pedersen, N. Brunner, and I. J. Christensen, *Lung Cancer* **51**, 193 (2006).
- <sup>9</sup>E. M. Bekes, E. I. Deryugina, T. A. Kupriyanova, E. Zajac, K. A. Botkjaer, P. A. Andreasen, and J. P. Quigley, *Neoplasia* **13**, 806 (2011).
- <sup>10</sup>WHO News Room/Fact Sheets/Detail/Cancer (2018), see <https://www.who.int/news-room/fact-sheets/detail/cancer>.
- <sup>11</sup>Y. Shao, J. Wang, H. Wu, J. Liu, I. A. Aksay, and Y. Lin, *Electroanalysis* **22**, 1027 (2010).
- <sup>12</sup>S. Pandit, "Graphene and graphene oxide based biosensors," *ResearchGate* (published online) (2015).
- <sup>13</sup>M. Pumera, *Mater. Today* **7–8**, 308 (2011).
- <sup>14</sup>C. I. L. Justino, A. R. Gomes, A. C. Freitas, A. C. Duarte, and T. A. P. Rocha-Santos, *Trends Anal. Chem.* **91**, 53 (2017).
- <sup>15</sup>C. Lu, H. Yang, C. Zhu, X. Chen, and G. Chen, *Angew. Chem.* **121**, 4879 (2009).
- <sup>16</sup>W. Yang, K. R. Ratnac, S. P. Ringer, P. Thordarson, J. J. Gooding, and F. Braet, *Angew. Chem. Int. Ed.* **49**, 2114 (2010).
- <sup>17</sup>Y. Wang, Z. Li, J. Wang, J. Li, and Y. Lin, *Trends Biotechnol.* **29**, 205 (2011).
- <sup>18</sup>J. H. Jung, D. S. Cheon, F. Liu, K. B. Lee, and T. S. Seo, *Angew. Chem.* **122**, 5844 (2010).
- <sup>19</sup>E. Morales-Narvaez and A. Merkoci, *Adv. Mater.* **24**, 3298 (2012).
- <sup>20</sup>A. Kasry, A. A. Ardakani, G. S. Tulevski, B. Menges, M. Copel, and L. Vykhlycky, *J. Phys. Chem. C* **116**, 2858 (2012).
- <sup>21</sup>Z. Chen, S. Berciaud, C. Nuckolls, T. F. Heinz, and L. E. Brus, *ACS Nano* **4**, 2964 (2010).
- <sup>22</sup>S. Eustis and M. A. El-Sayed, *Chem. Soc. Rev.* **35**, 209 (2006).
- <sup>23</sup>P. K. Jain, X. Huang, I. H. El-Sayed, and M. A. El-Sayed, *Plasmonics* **2**, 107 (2007).
- <sup>24</sup>R. M. Williams, C. Lee, and D. A. Heller, *ACS Sens.* **3**, 1838 (2018).
- <sup>25</sup>B. Sharma, S. Chiluwal, and R. Podila, *Nanoscale* **11**, 14010 (2019).
- <sup>26</sup>B. Saha, T. H. Evers, and M. W. Prins, *Anal. Chem.* **86**, 8158 (2014).
- <sup>27</sup>T. C. Ta and M. T. McDermott, *Anal. Chem.* **72**, 2627 (2000).
- <sup>28</sup>M. Lundqvist, J. Stigler, G. Elia, I. Lynch, T. Cedervall, and K. A. Dawson, *Proc. Natl. Acad. Sci. U.S.A.* **105**, 14265 (2008).
- <sup>29</sup>S. Grimme, *J. Comput. Chem.* **27**, 1787 (2006).
- <sup>30</sup>S. Grimme, J. Antony, S. Ehrlich, and H. Krieg, *J. Chem. Phys.* **132**, 154104 (2010).
- <sup>31</sup>S. Grimme, S. Ehrlich, and L. Goerigk, *J. Comput. Chem.* **32**, 1456 (2011).
- <sup>32</sup>J. R. Lakowicz, *Anal. Biochem.* **298**, 1 (2001).
- <sup>33</sup>K. H. Drexhage, *Progress in Optics*, edited by E. Wood (North Holland, Amsterdam, 1971), p. 161.
- <sup>34</sup>W. L. Barnes, *J. Mod. Opt.* **45**, 661 (1998).
- <sup>35</sup>R. M. Amos and W. L. Barnes, *Phys. Rev. B* **59**, 7708 (1999).
- <sup>36</sup>See supplementary material at <https://doi.org/10.1116/1.5128889> for Figs. S1–S7.